Development of a piezoelectric actuator for trailing edge flap control of full scale rotor blades

To cite this article: F K Straub *et al* 2001 *Smart Mater. Struct.* **10** 25

INSTITUTE OF PHYSICS PUBLISHING SMART MATERIALS AND STRUCTURES

Smart Mater. Struct. **10** (2001) 25–34 www.iop.org/Journals/sm PII: S0964-1726(01)20358-9

Development of a piezoelectric actuator for trailing edge flap control of full scale rotor blades†

F K Straub, H T Ngo, V Anand and D B Domzalski

The Boeing Company, Mesa, AZ 85215, USA

Received 6 August 1999, in final form 28 November 2000

Abstract

The present paper covers the development of a piezoelectric actuator for trailing edge flap control on a 34 ft diameter helicopter main rotor. The design of an actuator using biaxial stack columns, and its bench, shake, and spin testing are described. Actuator bench testing proves the basic actuator concept, but also points to required performance improvements. Actuator robustness is demonstrated in shake and spin tests simulating the full range of dynamic conditions inside the rotor blade. A series of actuator improvements are implemented, resulting in almost doubled performance. Projections using the latest stack technology show that the improved actuator will meet the performance requirements. The next steps in this program are development of the actuator and full scale rotor system for whirl tower testing and flight testing on the MD Explorer.

(Some figures in this article are in colour only in the electronic version; see www.iop.org)

1. Introduction

Piezoelectric actuators have been used successfully in a number of applications, primarily in the areas of micro-positioning. Examples include acoustic transducers, adaptive optics, and printer technologies. Piezoelectric driver elements allow the construction of all-electric actuators of compact design with few parts and a minimum number of moving parts that offer high bandwidth and high precision. Recent advances in piezoelectric materials now make it possible to consider macro-positioning applications that require large stroke and force. Applications that are being targeted include the active control of vibration and noise in machine tools, aircraft, spacecraft, and marine vehicles.

Helicopters typically experience high levels of vibration and noise, as a result of the unsteady aerodynamic and dynamic environment that the main rotor operates in during forward flight. Conventional approaches, such as design optimization and vibration absorbers, have shown only limited effectiveness. The active control of rotor vibrations using high bandwidth hydraulic actuators in the control system has been successfully demonstrated. However, it has not been implemented because of its complexity and cost, as well as safety concerns. For maximum effectiveness, one would like to cancel or reduce the unsteady forces close to the source; that is, directly on the rotor blade. At the same time, such on-blade control is of limited authority and independent of the primary flight controls, and thus inherently safe. In principle, it can be achieved by changing the rotor blade twist or airfoil shape, including the use of trailing edge flaps and leading edge slats.

Several piezoelectric actuation schemes are currently being developed to effect rotor blade active control. The piezoelectric material can be directly imbedded into the structure, in the form of sheets [1] or fibers [2]. In this case the inherent stiffness of the blade structure has to be overcome, which poses a significant challenge for blade twist changes and may be prohibitive for camber and thickness changes. In addition, blade structural integrity and life issues must be carefully considered. The piezoelectric material can also be constructed into discrete actuators that are mounted inside the blade and drive hinged control surfaces [3–8]. This approach allows for the maintenance and replacement of actuators, has only limited impact on blade structural integrity, and isolates the piezoelectric elements from high blade strains and stresses. More importantly, using aerodynamic leveraging, the control surfaces can be designed to minimize the actuation requirements and maximize the aeroelastic effectiveness. Furthermore, this modular approach lends itself to testing alternative actuator concepts, as long as envelope, mass, and power constraints are met.

† Presented at SPIE's Symposium on Smart Structures and Materials, Paper Number 3668-104, Newport Beach, 1999.

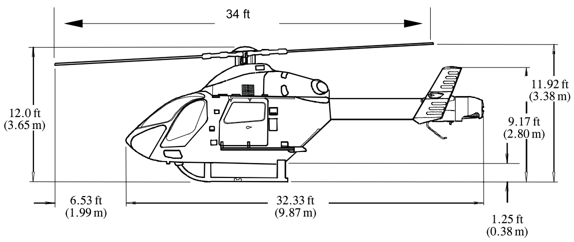

Figure 1. The MD Explorer light utility helicopter.

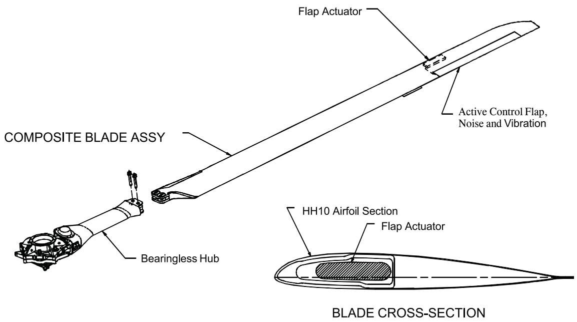

Figure 2. Blade with trailing edge flap and piezo stack actuator.

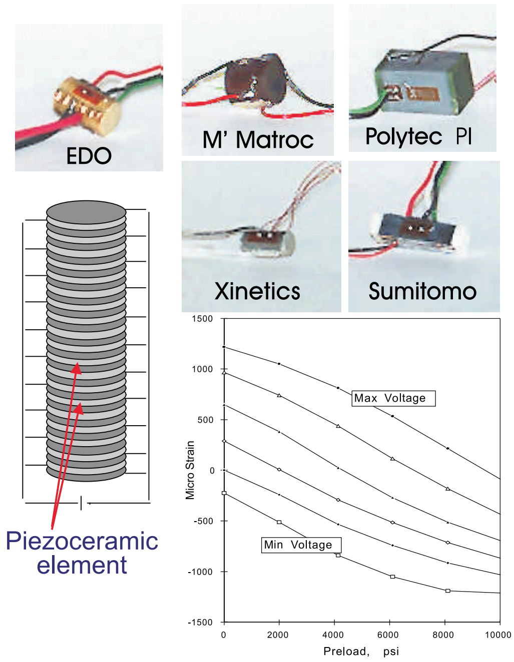

Figure 3. Piezoelectric stacks tested and typical result.

A previous study [4] described the conceptual sizing and design of a full scale active control demonstration system for the MD Explorer helicopter, figure 1. This modern, twin-turbine, 6000 lb, eight-seat helicopter has a 34 ft diameter composite, bearingless main rotor with five blades of 10 inch chord. For the present program, an integral flap spanning from 74% to 92% radius, figure 2, is used for high bandwidth active control functions including vibration and noise reductions, and aerodynamic performance improvements. It is driven by a piezoelectric actuator that is mounted inside the blade spar, figure 2. The flap aeromechanical design parameters are tailored to minimize the actuation requirements [9]. This system provides a unique synergy between rotor aerodynamics and dynamics as well as smart materials. It is inherently simple, is all electric, has a low parts count, and is very modular and maintainable. Furthermore, the system is of limited authority and completely independent of the primary flight controls, thus it is inherently safe.

The overall objectives of this DARPA sponsored program are to demonstrate the feasibility of using smart materials for helicopter active control and to evaluate the performance and cost benefits. The projected results and payoffs from rotor blade active control are significantly improved component lives and reduced maintenance, as well as improved crew, passenger, and community acceptance. The specific design goals in the individual areas are as follows. (1) Vibrations, an 80% reduction in airframe vibrations with resulting significant improvements in ride quality, component reliability and life, and maintenance. (2) Acoustics, a 10 dB reduction in blade vortex interaction (BVI) noise while landing. (3) Aerodynamic performance, a 10% gain in rotor performance (lift/drag) and improved maneuverability from stall alleviation.

The specific issues addressed in the present paper are: (1) the testing and selection of piezoelectric stacks; (2) the design and fabrication of a piezoelectric actuator; (3) bench, shake, and spin testing of the actuator with PI stacks; and (4) actuator improvement.

2. Piezoelectric actuation

Piezoelectric materials have limited strain capability. Commercially available materials offer strains of about 0.1%, state-of-the-art materials have about 0.2% strain output, and now emerging single-crystal ceramics promise up to 0.5% strain but may have a reduced modulus of elasticity. For application in discrete actuators, several methods are available to construct ceramic actuator elements from the basic ceramic material; these include multilayer stacks, bimorphs, C-blocks, Rainbow, Thunder, and tubular [10]. These actuator elements use different modes of operation, i.e. normal, shear, and torsion, and may have inherent amplification mechanisms that trade force for stroke output. In general, several actuator elements (of one type) are added together to increase the stroke and/or force output. They are then combined with a mechanical system to provide mounting and output connections, isolation from undesirable external forces and environmental effects, and possibly additional leveraging.

For rotor blade trailing edge flap control, stacks [4–6], bimorphs [3, 7], and C-block [8] actuator elements have been proposed. The highest mechanical work density has been reported for monolithic multilayer d_{33} actuator elements [11]. Such stacks are chosen for the current application. Although stacks are available from a number of manufacturers, information on stack performance under combined electrical and mechanical loading is generally lacking. Stacks from Morgan Matroc, Physik Instrumente (PI), Xinetics (Xi), EDO, Sumitomo (Su), and the Rockwell Science Center (RSC) were tested, figure 3. A total of 11 stack samples were tested, including different materials for some of the manufacturers, as well as low- and high-voltage stack

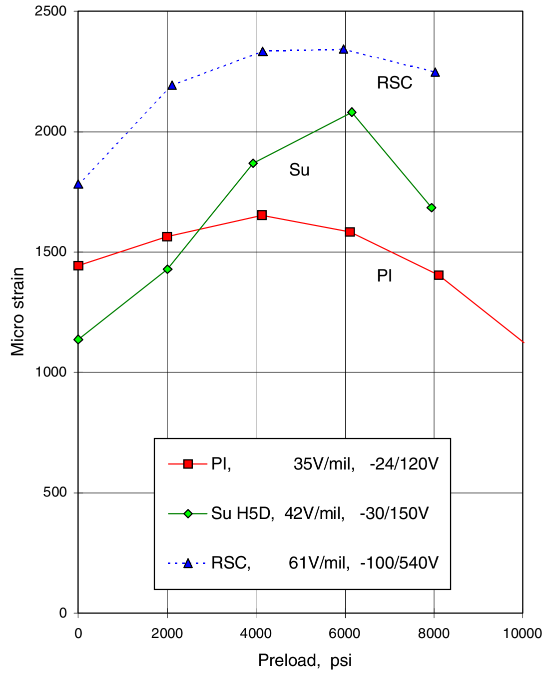

Figure 4. Piezo stack strain comparison (PI, Su, RSC).

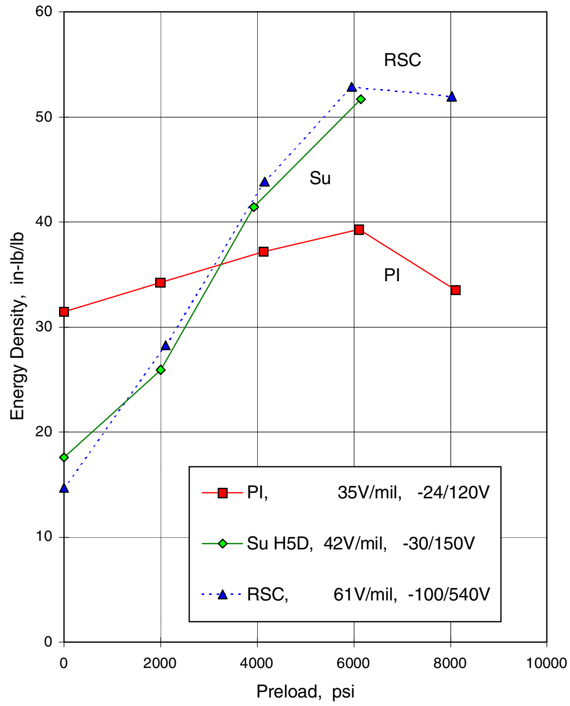

Figure 5. Piezo stack energy density comparison (PI, Su, RSC).

construction. The test objectives were to determine the stroke and the modulus for each stack under a range of representative loads and select the best stack for the current application based primarily on energy density.

Stacks were tested under a range of mechanical preloads (0–10 000 psi) using dc and ac drive voltages [12]. From this, the stack strain and elastic modulus were determined, as well as a number of derived parameters, including the

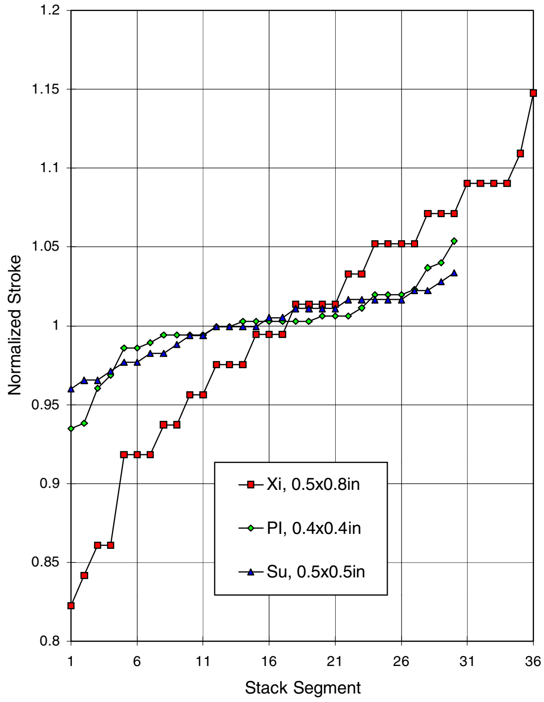

Figure 6. Normalized stroke distribution for stack segments (XI with 36 segments and PI and Su with 30 segments).

energy density. Results are presented for the PI, Su, and RSC stacks when using dc voltages. The PI and Su stacks use PZT formulations, whereas the RSC stack uses a PLZT formulation. The strain output and energy density for the three stacks are shown for manufacturer recommended voltage ranges of 144, 180, and 640 V (peak to peak), respectively, corresponding to field levels of 35, 42, 61 V/mil layer thickness. Figure 4 shows the strain output against applied preload. The PI stack exhibits a modest change in strain with preload, with a maximum of 1650 microstrain at 4000 psi. The Su stack shows greater variation of strain with preload, with a maximum of 2080 microstrain at 6000 psi. The RSC stack has the highest strain output of the three, with a maximum of 2340 microstrain at 6000 psi. The strain, modulus, and density are used to derive the energy density ($\frac{1}{2}\varepsilon^2 E/\rho$) for each stack. Note, however, that the test procedure resulted in an overestimation of the modulus. Thus, the results for the energy density should only be used to compare the relative merits of the three stacks. Figure 5 shows the PI stack with only a small variation of energy density against preload, which is desirable for applications where a wide range of load is expected, such as in helicopter active control. The Su and RSC stacks have a significant variation of energy density against preload, but their maximum energy density is about 40% greater than that of the PI stack.

For the prototype actuator development, off-the-shelf stacks from PI (P-915.858) and custom stacks from Su (PSA-15C-12SN-H5D) were selected, since the RSC stack had the same energy density as the Su stack, but required a high voltage drive. 30 stacks were ordered from each manufacturer. Figure 6 shows the free stroke for each stack, normalized by the average stroke of the respective set. The Su and PI stacks have a variation of up to 4% and 7% from the average stroke, respectively, which is indicative of the maturity of their stack manufacturing process. During the initial stages of this program when developing large cross section cofired stacks [13], variations up to 18% were seen for 36 Xi stacks, figure 6. Each stack was also subjected to burn-in at a nominal ac voltage for 10^5 cycles. During this process, a few of the Su stacks shorted out, requiring reduced drive voltages during later actuator testing. This shorting may have been caused by using thinner endplates than usual, which led to minor irregularities in the insulating coating near the end.

3. Actuator design and fabrication

Actuator design is driven by the required mechanical output, envelope and weight constraints, and the dynamic operating environment. The force and stroke requirements are based on aeroelastic simulations for vibration reduction at 145 knots level flight. At a minimum, 28 ± 43 lb force at a stroke of ± 0.032 in are required. Later versions, using high-output single-crystal stacks, are expected to provide 41 ± 63 lb and ± 0.062 in. These two cases correspond to $\pm 2^\circ$ and $\pm 4^\circ$ of nominal flap deflection, using a flap horn length of 0.75 in. (Note that the required actuator strokes account for losses incurred between the flap and the actuator as well as flap elastic twist and are thus higher than the nominal flap deflections.) These flap deflections, because of the large flap size, provide a significant amount of change in blade lift and moment, and thus control authority. For installation inside the blade spar the actuator envelope is limited to a cross section of approximately 0.7×2.0 in and the total length is not to exceed 20 in. The target weight is 2 lb or less. Note that the allowable actuator weight is also a function of its chordwise center of gravity location. To meet aeroelastic stability considerations, the installation of the actuator close to the airfoil leading edge is beneficial. The actuator must maintain full authority under steady radial acceleration of $655g$ (nominal at 150 in radius), and level flight vibratory flapwise and chordwise accelerations of $29g$ and $3g$, respectively. Some performance degradation is allowed under maneuvering flight accelerations of $49g$ (flapwise) and $27g$ (chordwise). The actuator must maintain integrity under $851g$ (radial), $83g$ (flap), and $56g$ (chord).

The actuator bandwidth should be greater than 40 Hz (6/rev), with a phase lag of less than 10° at 40 Hz. The actuator resolution and position sensing accuracy should be 3% or less of the full range. The ambient operating temperatures ranges from -60 to 160 °F. Humidity levels of up to 100%RH may be encountered. In case of a failure, the actuator should return to the mid-travel position. An actuator life of 4500 h mean time between failures (MTBF) under a 100% duty cycle is desired. A maximum stack voltage of less than 200 V is preferable. Some of these requirements need not be met by the prototype actuator or during initial demonstration. They are presented here for completeness.

The actuator design is based on a parallel arrangement of two long stack columns in the blade spanwise direction [13]. The stacks operate out of phase in a push–pull mode and thus apply a moment to the short leg of an L-shaped lever, figure 7. This lever takes the form of a tubular beam (gusset) that is closed off at its inboard end. The gusset is supported at its inboard end by means of a flexural mount. This mount allows

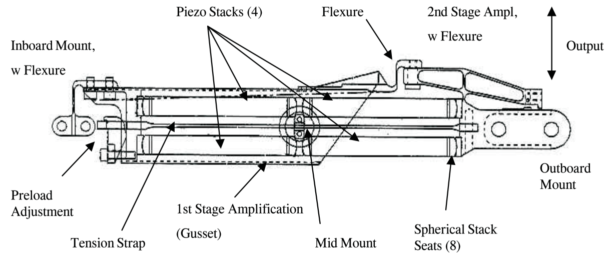

Figure 7. Schematic diagram of the biaxial piezoelectric flap actuator.

for collective (in-phase) extension of the stacks and relative spanwise motion between the actuator and the blade. It also allows the gusset to pivot angularly about a virtual hinge point at the center of the mount. Both stacks are nestled within the gusset. The inboard end of both stacks reacts against the inside end of the gusset. Differential (out of phase) extension of the stacks causes an angular motion of the gusset. Sufficient clearance is provided between the gusset and stacks to allow for unconstrained rotation. The gusset represents the first stage of stroke amplification where the output motion occurs at its outboard end in a direction perpendicular to the stack axes. The length of the gusset from the center of the inboard flexure mount to the output point divided by the center-to-center distance between the stacks defines the amplification ratio. The power-off position of the actuator and the mid-point of the actuator stroke are nominally the same. This point is affected by geometric tolerance variations, and could be adjusted by changing the length of one stack column using shims. In the current actuator, a jack screw located in the closed end of the gusset (not shown) is used to adjust the length of the aft stack column. It can be used to conveniently center the actuator, compensate for tolerances, or to introduce a bias displacement.

The outboard end of both stack columns reacts against a rigid mount which is fastened to the rotor blade, figure 7. This mount transmits the actuation forces and actuator spanwise inertial forces to the blade. Integral with this mount is a second-stage amplification lever. This lever has an I-beam type cross section and is pivoted near its center, providing a modest amount of amplification. The fulcrum of this lever consists of a flexure integral with the beam and the outboard mount. The output of the first stage is fastened to the input (inboard end) of the second stage. An additional flexure on the first stage allows for relative motion between the two stages due to foreshortening. The outboard end of the second stage is connected to the load link that transmits the actuator output to the flap. The output displacement is measured using a Hall sensor on the outboard mount and a magnet on the second stage. The output force is measured using strain gages on the load link.

Piezoelectric stacks must always operate in compression, since they have very low tensile strength. A tension strap, located between the two stack columns, is attached to the outboard mount at one end and to the gusset inboard end using a toggle lever and screw, figure 7. The total preload in the stacks is a combination of the mechanical preload, applied by tensioning the strap via the lever, and the additional preload arising from applying a dc bias voltage to both stacks. The

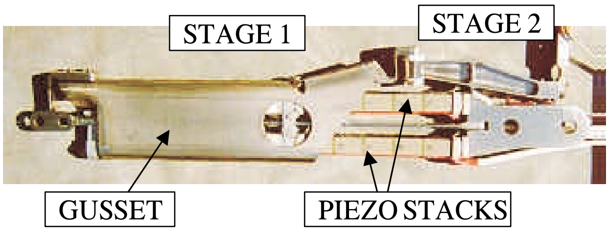

Figure 8. Photograph of the biaxial piezoelectric flap actuator.

preload can easily be adjusted to values where the stacks will perform optimally. All stacks have spherical end caps and corresponding spherical sockets in the mounts. These seats allow for a pivoting motion, they isolate the stacks from any externally applied moments, and facilitate the centering of the stacks during assembly. They also restrain the stacks against transverse inertial loads and have the advantage of zero freeplay and high stiffness under preload.

The biaxial arrangement of stacks provides a number of advantages compared to other actuators. First, no actuator reaction structure is required, thus reducing the actuator weight and maximizing the available volume for stacks. Second, thermal expansion does not cause actuator output. Third, the required preload spring does not reduce output, since the stacks are operated differentially. Last, the power-off position corresponds to zero flap deflection. Flexures are used throughout the actuator to eliminate freeplay associated with bearings. Adjustments are provided to account for blade stretch, tolerance buildup, and preload stretch in order to minimize flexure operational deflections and the resulting stresses. These flexures do, however, represent either a parallel stiffness or an in-series compliance that reduce the available actuator output. The slenderness of the actuator allows placement forward of the blade quarter chord, thus contributing to dynamically balance the blade, and thereby reducing the amount of balance weight required.

Practical limitations are imposed on the actuator stroke amplification. As the amplification ratio increases, the mechanism size and weight increase, its flexibility increases, and the effect of lost motion in the inner stages is amplified. At the same time limitations are imposed on the length of the stack columns, considering buckling under preload and bending due to transverse inertia loads. To meet the current design requirements, a mid-mount is introduced. Thus four stacks are now used, each being half the original length, requiring four additional spherical end caps and sockets, figure 7. A mid-mount supports the stacks in the blade, without impeding stack extension or gusset motion. The mount has a rigid centerpiece, which contains four sockets to seat the stacks, and is connected to the blade with upper and lower aluminum/elastomeric laminates. Each laminate has opposing aluminum disks with several intermeshing ridges, which are shaped to make the laminate soft with respect to stack collective and differential extension, but stiff with respect to in- and out-of-plane motions.

The inboard mount, gusset, outboard mount, second stage, and load link are made from titanium; steel is used for all other parts. All flexures are machined using wire EDM. Two half-shells are formed from sheet stock and are welded together with two inserts to make the gusset, thus ensuring maximum stiffness. Five stack segments of 18 mm length each are bonded together and fitted with spherical end caps to form one of the four stack columns. The stack cross section is 10×10 mm^2 for the PI stack and 12.7×12.7 mm^2 for the Su stacks. To facilitate assembly, the four stacks and the mid-mount centerpiece are bonded together in a fixture using elastomer. This subassembly is then slipped inside the gusset, the tension strap is inserted and the in- and outboard mounts are attached. Last, the connection of the first and second stages is made. The actuator and load link are shown in figure 8. The total stroke amplification is about 10; 8.4 for the first stage and 1.2 for the second stage. The nominal preload (mechanical and 50 V dc) of the stacks is approximately 3100 psi. The total weight of the PI stacks is 0.62 lb for a total actuator weight of 1.65 lb. The total actuator weight with Su stacks is 2.03 lb.

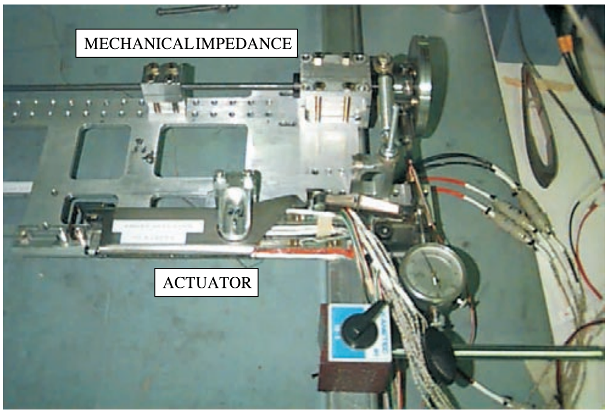

Figure 9. The flap actuator and bench test rig.

4. Actuator testing

4.1. Test set-up

The actuator is tested on a rig that provides an adjustable mechanical impedance. The actuator and loading device are mounted on a base plate. The actuator load link is connected at an offset to a torsion bar spring. The stiffness of the torsion bar spring can be varied by clamping it at different lengths, from spanning free stroke to nearly blocked force type conditions. A number of disks are attached to the torsion bar to simulate the flap inertia. A friction clutch can be spring loaded to provide damping. The fitting of the mid-mount disks and final adjustments are made on the actuator bench test rig, figure 9. The actuator is driven using an existing, modified linear amplifier, to provide two channels of 150 Vpp (peak-to-peak voltage) at 6 A nominal each. The amplifier itself is powered by several high- and low-voltage, off-the-shelf power supplies. The actuator voltage is controlled by selecting the dc level and providing an ac command. The ac command is inverted in the amplifier to drive the second channel. All tests are conducted using sinusoidal ac commands. For the basic bench, shake, and spin testing PI stacks are used. Su as well as PI stacks are used during the actuator improvement testing.

A VXI-based data system is used to record 18 channels of mechanical and electrical data. In general, a sampling rate of 1 kHz is used. The actuator stroke and force are measured using a Hall sensor, which is integral to the actuator, and a strain

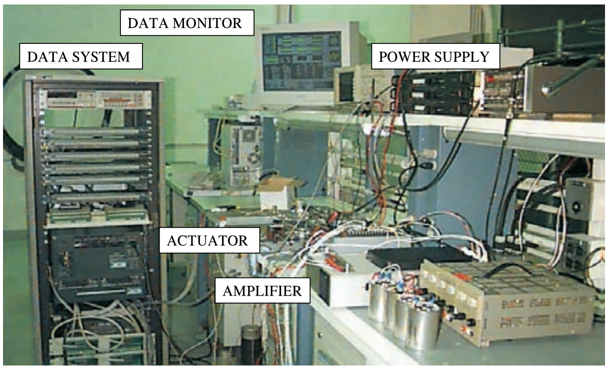

Figure 10. The bench test set-up.

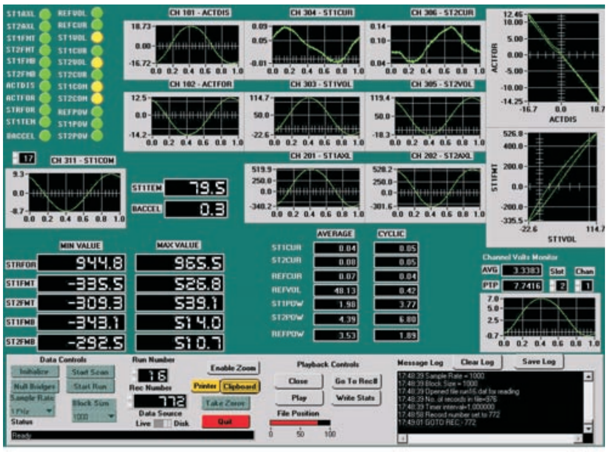

Figure 11. Data system monitor.

gage on the load link. The two outboard stack columns have one full and two half axial strain gage bridges each. The stack bending is derived from the two half-bridges in the middle of the stack columns. A strain gage on the tension strap is used to set and monitor the stack preload. The electrical data are the actuator ac voltage command, and the stack dc and ac voltages and respective currents. Finally, the stack temperature and actuator acceleration are also recorded. The entire bench test set-up is shown in figure 10. A PC-based system together with LabWindows is used for data monitoring, display, and processing. The display shows real time data, including several time history wave forms, hysteresis loops, statistical values, and warning lights indicating safety limit exceedances, figure 11.

4.2. Bench testing

Actuator basic performance with the PI stacks is obtained by driving it at 1 Hz using seven voltage levels, from 20 to 144 Vpp, and eight different external stiffness values, i.e. torsion bar lengths. Figure 12 shows the actuator force against displacement at different voltage levels. The actuator output increases almost linearly with the peak-to-peak voltage, indicating that the stacks are operating well below saturation. The actuator output also changes almost linearly with the external spring stiffness; somewhat higher output is seen at very soft and very stiff conditions. The actuator performance against frequency up to 40 Hz (about 6/rev for

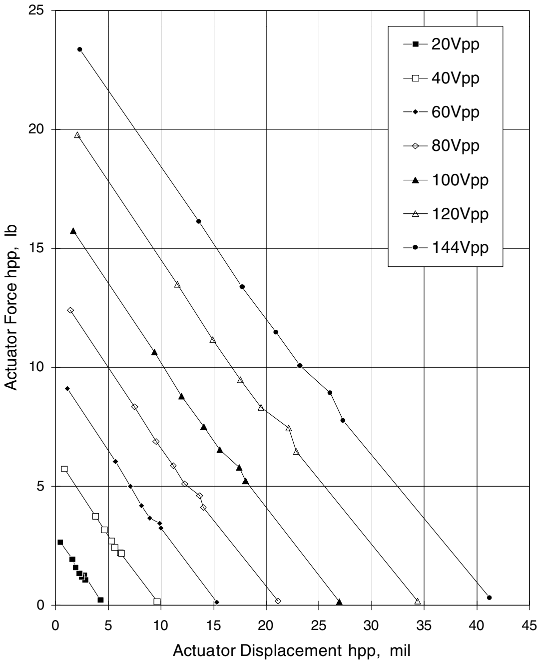

Figure 12. Force–displacement characteristics (20–144 Vpp, 1 Hz, PI stacks).

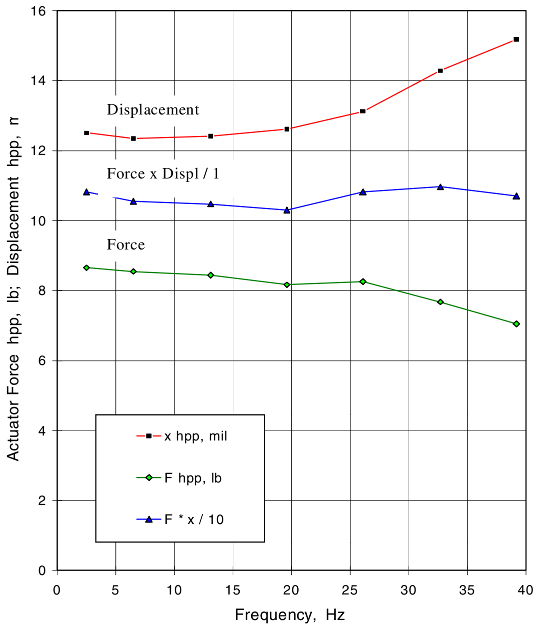

Figure 13. Actuator performance against frequency (100 Vpp, 750 lb in^{-1}, PI stacks).

the MD900) is evaluated at 100 Vpp and 750 lb in^{-1} external stiffness. Figure 13 shows that the stroke increases and the force decreases with frequency, although the product remains approximately the same. Frequency sweeps show the lowest actuator mode to be above 250 Hz. With the actuator connected to the impedance rig, the lowest modes are 81 and 97 Hz for external stiffness values of 750 and 1180 lb in^{-1}, respectively.

The actuator performance under blade elastic deformations was evaluated by shimming the in- and outboard mounts to simulate either out-of-plane bending or torsional blade de-

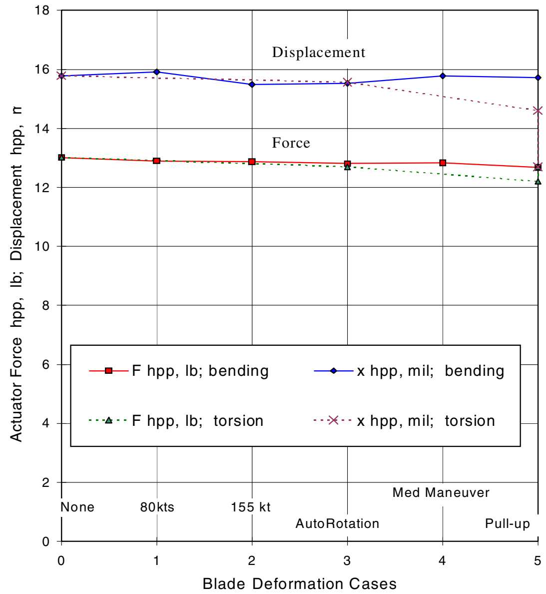

Figure 14. Actuator performance under simulated blade deformations (144 Vpp, 1 Hz, 750 lb in^{-1}, PI stacks).

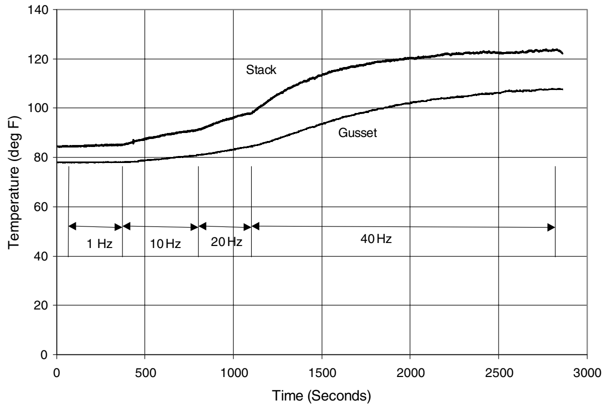

Figure 15. Stack temperature profile (100 Vpp, 40 Hz, PI stacks).

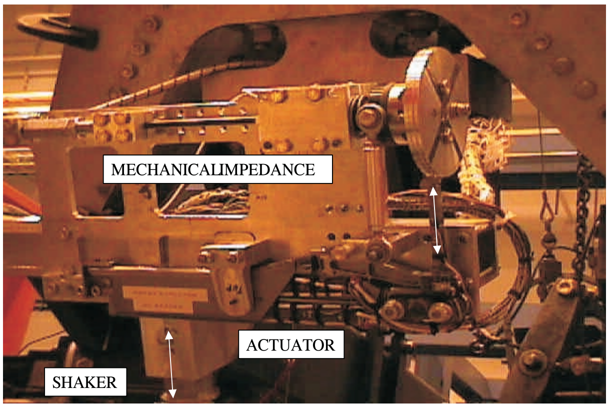

Figure 16. Actuator and bench test rig during shake test, plan view.

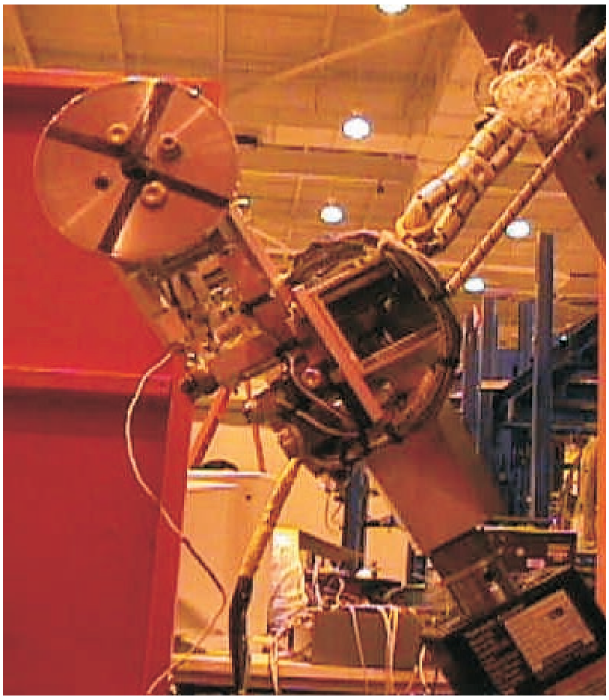

Figure 17. Actuator and bench test rig during shake test, side view.

formations. Aeroelastic simulations were run to predict the maximum blade elastic deformations at 80 and 155 knot level flight, at 150 knot, 1.75g autorotation, at moderate pull-up, and at 150 knot, 2.75g pull-up conditions. The appropriate shim values were derived from blade bending curvature and twist rates. The actuator performance against increased shimming is evaluated for 144 Vpp at 1 Hz, 750 lb in^{-1} torsion bar stiffness, and a small amount of damping. Figure 14 shows that the stroke and force output remain nearly unchanged. Only for the highest value of torsional deformation is the output somewhat reduced, indicating that the actuator may be somewhat more sensitive to blade torsional deformation. Evaluating actuator performance under blade in-plane bending deformations was not possible. However, when displacing the inboard mount to the maximum in-plane deformation, no significant actuator output was observed.

Additional tests included the variation of the stack preload, which did not measurably affect performance. The stack temperature during extended performance was evaluated by running the actuator on the bench at 100 Vpp and several frequencies. The results showed that the stack heating rate was proportional to frequency. For 40 Hz operation, the stack temperature stabilized at about 40 °F above ambient, figure 15. The figure shows the gusset temperature to be about 10 °F lower than stack temperature (not including an erroneous offset under ambient conditions). Actuator heating is not expected to be a problem since the rotor blade moves at 510 ft s^{-1} at the point of actuator installation, and air moves through the blade spar due to centrifugal pumping.

4.3. Shake testing

The actuator with PI stacks was shake tested to demonstrate performance under level flight vibratory out-of-plane and in-plane motions, as well as to demonstrate actuator integrity under maneuver vibratory motions. To provide oscillatory base motion, the bench test rig and actuator were mounted on a hydraulic shaker, first for flapwise and then for chordwise

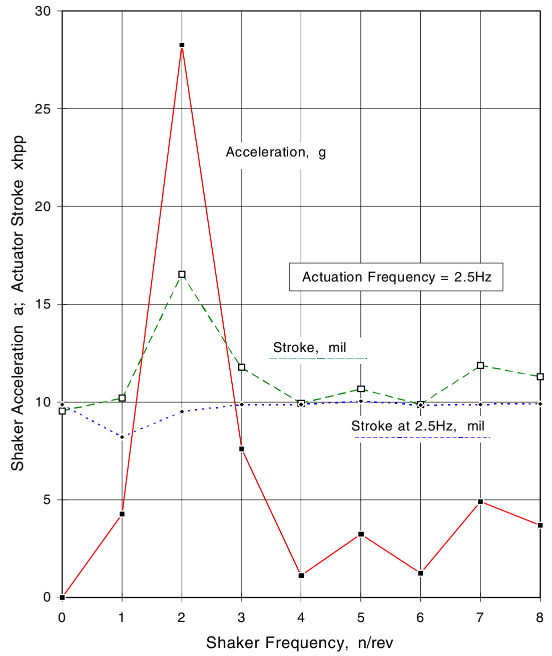

Figure 18. Actuator performance under out-of-plane base motion (100 Vpp, 2.5 Hz, 750 lb in^{-1}, PI stacks).

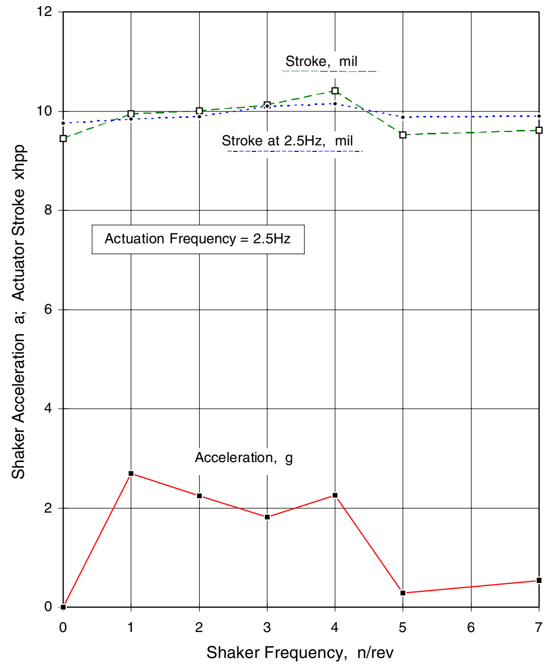

Figure 19. Actuator performance under in-plane base motion (100 Vpp, 2.5 Hz, 750 lb in^{-1}, PI stacks).

motions. The torsion bar stiffness was set to 750 lb in^{-1}, and a small amount of damping was added. Figures 16 and 17 show the shake test set-up in plan and side views, with the bench test rig mounted for chordwise shaking. Acceleration levels at rotor speed multiples were based on aeroelastic simulations. Before shake testing, the actuator components were loaded statically to the maximum g-level loads, in order to ensure integrity. Furthermore, a restraint and second Hall sensor were added to limit the loading of the second-stage flexure and to measure the out-of-plane motion at the actuator output. During the shake test the actuator was tested at the full range of command voltages and frequencies.

Results are presented for actuator inputs at 100 Vpp and 2.5 Hz while varying the shaker frequency from 1/rev (6.5 Hz) to 8/rev using level flight g levels. Figure 18 shows actuator stroke and flapwise g levels (29g maximum at 2/rev) against shaker frequency. The actuator stroke at the command 2.5 Hz is essentially unaffected by the flapwise base motion. However, the overall stroke output increases in proportion to the base motion g level. This is attributable to the bench test rig mounting plate being relatively soft in the out-of-plane direction. Statically loading the torsion bar bearing in the flapwise direction indeed produced an output of the actuator that was in accordance with above observation. Figure 19 shows actuator stroke and chordwise g levels (2.7g maximum at 1/rev) against shaker frequency. The overall actuator stroke and its 2.5 Hz component are rather similar, as expected, since the mounting plate is very stiff in-plane, and both are essentially unaffected by the chordwise base motion. The actuator was also subjected to full maneuver g levels (except at 1P chordwise and 2P flapwise), and it maintained its integrity.

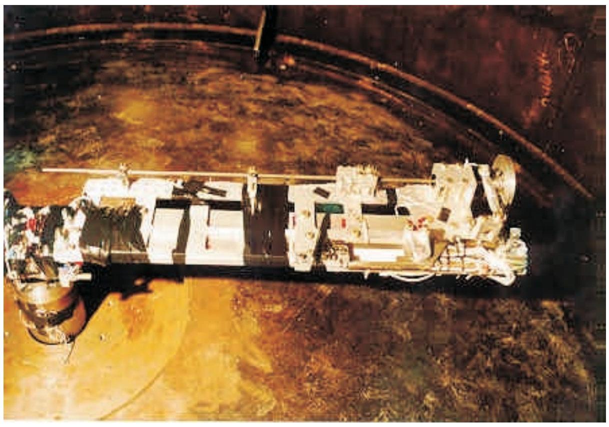

Figure 20. Actuator and bench test rig during spin testing.

4.4. Spin testing

The actuator with PI stacks was spin tested to demonstrate the performance in the rotating system under full centrifugal loads. The University of Maryland vacuum spin chamber was used to provide realistic loading of all actuator components. The bench test rig and actuator were mounted on a rotating, counter-balanced beam, figure 20. Since the radius was limited to less than 5 ft, the rotor speed was increased to simulate full centrifugal force (CF) loading. The torsion bar stiffness was set to 750 lb in^{-1}, without any damping added. Furthermore, the torsion bar bearing was restrained to the bearing block. To provide additional safety, a lightweight load link was used together with a simple roller bearing to prevent excessive bowing of the load link under CF loading. The actuator was then tested at the full range of command voltages and frequencies for a range of rotor speeds up to its nominal value (627g at 143.6 in). The actuator was also run at 20 Vpp and

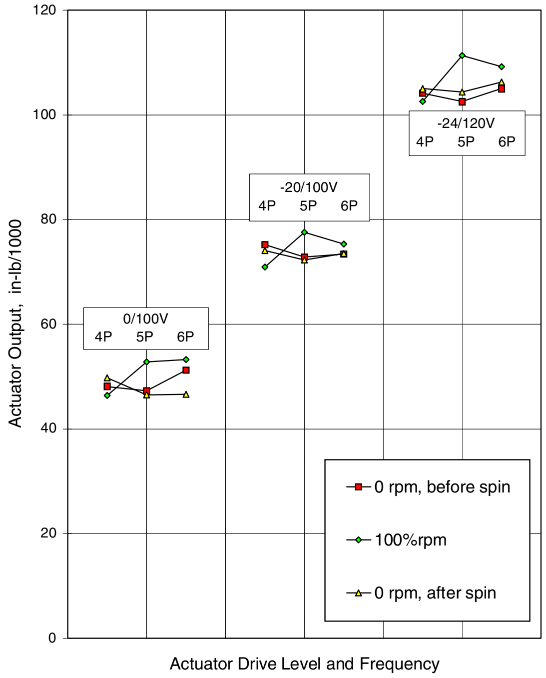

Figure 21. Actuator performance during spin testing (627g) and after overspeed to 814g (750 lb in^{-1}, PI stacks).

2.5 Hz at overspeeds up to 114% of nominal (814g). Figure 21 shows the actuator output (force × stroke) before spinning, at 100% rotor speed (627g), and after spinning. The voltage levels are 100, 120, and 144 Vpp at 4, 5, and 6/rev. The actuator output is essentially unchanged. A small increase in output at 100% rotor speed may be attributable to CF loading tightening-up the actuator and increasing the stack preload.

4.5. Actuator improvements

The actuator output seen in the initial bench testing was less than expected, leading to an effort to better understand and improve its performance. At first, the Su stacks were used in the actuator. Despite their greater energy density (figure 5) and cross section (60%), the output was less than with the PI stacks, primarily because they could safely be run at only 80% of their design voltage (144 Vpp instead of 180 Vpp), figure 22. For comparison, the results for an earlier prototype actuator [13] and the double x-frame actuator [14] are also shown in figure 22.

Next, detailed measurements were made of the motion of various actuator components and their stiffness, together with some finite-element modeling. From this it became apparent that the flexures of the second stage and between the two stages represented a significant parasitic stiffness. Thus, the actuator with the Su stacks (one segment inoperable) was run in a single-stage configuration, with an extended gusset of 12.5 amplification ratio to mate up to the original two-stage load link location. This more than doubled the free stroke, figure 22. When restraining the out-of-plane motion of this long gusset at its output, the blocked force was increased by 40%, figure 22.

Additional insight was gained by testing the stiffness of the actuator with strain gaged, aluminum and steel dummy stacks. Furthermore, based on simple analysis, the spherical stack

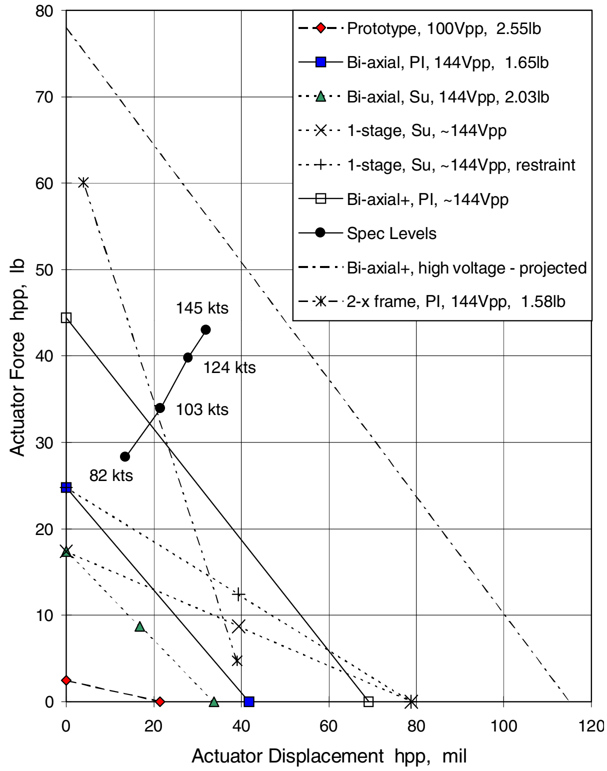

Figure 22. Actuator performance improvements.

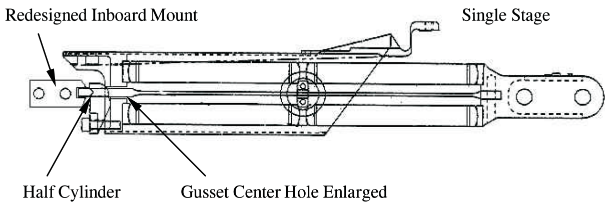

Figure 23. Improved actuator, biaxial+.

seats, which used different radii for the end cap and socket, represented a significant compliance. This was confirmed by measuring the spanwise displacement of the gusset under stack dc voltage and comparing the tension strap and stack strains. As a result, the sockets were changed to match the stack end-cap radius. At the same time the sockets were lined with a bearing material to keep friction, and thus stack bending, to a minimum. Last, the inboard flexure mount not only presented parasitic stiffness, it also contributed to lost motion. In its place, the inboard end of the tension strap was restrained in a tight fitting, slotted mount with the gusset pivoting directly against the strap/lever interface using a half-cylinder seat, figure 23. Also, the gusset/tension strap clearance was increased on account of the larger gusset rotations. Using the original short gusset, this improved actuator (biaxial+) had an amplification ratio of 7.5. The actuator was driven with PI stacks. (Note that in the PI stack columns three segment interfaces had debonded after initial testing. During the repair one segment became inoperable.) Figure 22 shows that the biaxial+ actuator has substantially improved output, sufficient for vibration reduction at about 100 knot and comparable to the double x-frame actuator. As the figure shows, this is still short of the specification required. However, performance predictions show that with high-voltage stacks (3Msi, 2500 microstrain, 12.7 $\times$ 12.7 mm^2 cross section) that have recently become available the specification requirements at 145 knot will be exceeded. The figure also shows that amplification of the biaxial+ actuator should be changed to 5.4 in order to improve energy transfer.

5. Conclusions

The development of a biaxial piezoelectric stack actuator for use in rotor blade trailing edge flap control has been described. Stack segments from several manufactures were tested under combined electro-mechanical loading to establish a comprehensive data base. Stack selection was based largely on energy density. A light-weight actuator with four biaxial stack columns, a mid-mount, and two-stage stroke amplification was designed and fabricated. Actuator bench testing with PI and Su stacks proved the basic actuator concept, but also pointed to required performance improvements. The biaxial actuator robustness was demonstrated in a series of bench, shake, and spin tests, subjecting the actuator to the full range of dynamic conditions inside the rotor blade, including 814g steady and 29g vibratory loading. A series of experimental and analytical efforts identified areas for actuator improvement. Several of the improvements were implemented and resulted in an almost doubled performance. Projections show that with use of recently available high-voltage stacks, the performance requirements will be met. Plans now call for the development of actuators and the full scale rotor system for whirl tower testing and flight testing on the MD Explorer.

Acknowledgments

This work was supported by DARPA under contract DAAH04-95-C-0006 from the US Army Research Office. Dr Ephrahim Garcia is the DARPA program manager and Dr Gary Anderson is the ARO technical monitor. Their support and guidance is sincerely appreciated. Many discussions with Dr I Chopra of the University of Maryland (UM) proved to be very helpful. At UM, T Lee performed the piezo stack testing, and together with A Bernhard supported the actuator spin test in the UM vacuum chamber. At Xinetics, M Solomon developed the power amplifier modifications. The support of our colleagues in Mesa, particularly J Li, J Jette, R Gaddy, L Kildall, R Weisenburger, T Birchette, and D Kennedy greatly contributed to the successful completion of the tests and actuator improvements.

References

[1] Chen P C and Chopra I 1997 Wind tunnel testing of a smart rotor with individual blade twist control *J. Intell. Mater. Syst. Struct.* **8** 414–25

[2] Derham R C and Hagood N W 1996 Rotor design using smart materials to actively twist the blades *Proc. American Helicopter Society 52nd Ann. Forum (Washington, DC, June 1996)*

[3] Koratkar N A and Chopra I 1998 Analysis and testing of a Mach-scaled rotor in hover with piezoelectric bender-actuated trailing edge flaps *Proc. SPIE Symp. on Smart Structures and Materials (San Diego, CA, March 1998)*

[4] Straub F K and King R J 1996 Application of smart materials to control of a helicopter rotor *Proc. SPIE Symp. on Smart Structures and Materials (San Diego, CA, March 1996)*

[5] Prechtl E F and Hall S R 1997 Design of a high efficiency discrete servo-flap actuator for helicopter rotor control *Proc. SPIE Symp. on Smart Structures and Materials (San Diego, CA, March 1997)*

[6] Jaenker P 1997 Electro-mechanical characterization of high performance piezoactuators *Proc. SPIE Symp. on Smart Structures and Materials (San Diego, CA, March 1997)*

[7] Fulton M V and Ormiston R A 1998 Small-scale rotor experiments with on-blade elevons to reduce blade vibratory loads in forward flight *Proc. American Helicopter Society 54th Ann. Forum (Washington, DC, May 1998)*

[8] Clement J W, Brei D, Moskalik A J and Barrett R 1998 Bench-top characterization of an active rotor blade flap system incorporating c-block actuators *Proc. 39th AIAA Structural Dynamics and Materials Conf. (Long Beach, CA, April 1998)*

[9] Straub F K and Hassan A H 1996 Aeromechanic considerations in the design of a rotor with smart material actuated trailing edge flaps *Proc. American Helicopter Society 52nd Ann. Forum (Washington, DC, June 1996)*

[10] Near C D 1996 Piezoelectric actuator technology *Proc. SPIE Symp. on Smart Structures and Materials (San Diego, CA, March 1996)*

[11] Giurgiutiu V, Chaudry Z A and Rodgers C A 1995 Stiffness issues in the design of ISA displacement amplification devices: case study of a hydraulic displacement amplifier *Proc. SPIE Symp. on Smart Structures and Materials (San Diego, CA, March 1995)*

[12] Lee T and Chopra I 1999 Design and spin testing of an active trailing edge flap actuated with piezostacks *Proc. 40th AIAA Adaptive Structures Forum (St Louis, MO, April 1999)*

[13] Straub F K, Ealey M A and Schetky L 1997 Application of smart materials to helicopter rotor active control *Proc. SPIE Symp. on Smart Structures and Materials (San Diego, CA, March 1997)*

[14] Hall S R, Tzianetopoulou T, Straub F K and Ngo H 2000 Design and testing of a double x-frame piezoelectric actuator *Proc. SPIE Symp. on Smart Structures and Materials (Newport Beach, CA, March 2000)*